Progress In Electromagnetics Research M, Vol. 23, 207–227, 2012

THREE-DIMENSIONAL WEDGE DIFFRACTION CORRECTION DEDUCED BY THE STATIONARY PHASE METHOD ON THE MODIFIED EQUIVALENT CURRENT APPROXIMATION (MECA)

H. Gómez-Sousa*, J. Á. Martínez-Lorenzo, and O. Rubiños-López

Department of Signal Theory and Communications, University of Vigo, EI de Telecomunicación, Campus Universitario, E-36310 Vigo, Spain

Abstract—This paper presents a new method for computing fields diffracted by a wedge for the MECA formulation, which is valid not only for perfect electric conductors but also for lossy penetrable dielectrics. The method is based on the computation of a wedge correction matrix, which establishes a mapping function between fields incident at and diffracted by the wedge. The MECA method is based, in general, upon the oblique incidence of a plane wave at the interface between free space and lossy dielectric media. MECA reduces to the well-studied physical optics (PO) formulation in case of PEC (perfect electric conductor) scatterers. In this work, we consider a scenario involving diffraction caused by a plane wavefront incident on a wedge with flat faces and straight edge. The version of the stationary phase method for three-dimensional equivalent source distributions is employed to calculate the asymptotic contribution of the integration boundary along the edge of the diffraction wedge. This contribution of the critical boundary points is compared to the GTD (geometrical theory of diffraction) diffracted field in order to obtain the correction matrix by which the incident electric field vector is multiplied in MECA. As required to accomplish this comparison, the three-dimensional incident electric field is previously resolved into an edge-fixed coordinate system. Good agreement is demonstrated between full-wave method-of-moments (MoM) results and the results obtained by modifying MECA with our diffraction correction technique.

Received 18 November 2011, Accepted 18 January 2012, Scheduled 17 February 2012

* Corresponding author: Hipólito Gómez-Sousa (hgomez@com.uvigo.es).

1. INTRODUCTION

The modified equivalent current approximation (MECA) method [1, 2] has extended the asymptotic, high-frequency technique physical optics (PO) to lossy materials with a complex effective permittivity. In MECA the equivalent electric and magnetic currents are calculated based on the oblique incidence of a plane wave at the interface, together with a field decomposition into TE and TM components.

In contrast to full-wave methods, like the method of moments (MoM), the PO and MECA formulations do not require large amount of computational resources to solve, with a high degree of accuracy and efficiency, electrically large problems. Although these advantages are important, neither PO nor MECA are able to correctly evaluate the edge diffracted fields [3, 4].

In order to introduce edge diffraction in the PO formulation, the physical theory of diffraction (PTD) was developed by Ufimtsev [5, 6]. PTD uses additional current components, known as fringe currents, evaluated from the difference between the PO formulation and rigorous fields found from the solution of canonical diffraction problems.

There have been many proposals for correcting in efficient ways, without using Ufimtsev's concept of fringe currents, the fact that the PO integrals lead to incorrect edge diffracted waves. In some of these proposals, a version of the stationary phase method (SPM) is applied [3, 7, 8]. The SPM is a mathematical approach that makes use of a rapidly varying phase of the integrand. This phase variation results in a self-cancelling oscillation of the exponential factor of the integrand. The solution to the integral is asymptotically approximated by the contribution of certain critical points distributed over the surface of the scatterer. The phase variation is slower in the vicinity of these points. In diffraction analysis, the critical points of interest are located on the boundaries of the integration domain. Most of the published applications of the SPM to the electromagnetic analysis are either about integration in one dimension or are related to models based on purely numerical calculations [7, 8].

Umul eliminated the aforementioned diffraction defect of PO by modifying its mathematical structure according to three axioms in the two-dimensional case [9]. In Section 5.6 of [3], James proposed multiplicative scalar correction factors obtained by the one-variable SPM in a two-dimensional edge diffraction problem where a PEC (perfect electric conductor) scatterer is considered. Sakina et al. studied a modification of a line integral reduction of PO [10]. In [11], Shijo et al. presented PO diffraction coefficients obtained by applying the one-variable SPM in the two-dimensional PEC case. Then they

defined modified surface-normal vectors which turn the PO diffraction coefficients into those of the GTD (geometrical theory of diffraction). They introduced empirical weights for the extension to the three-dimensional case.

In this work, we present a correction matrix which extends in three ways the aforesaid edge diffraction results reported by James in Section 5.6 of [3]. We employ a three-dimensional version of the SPM on a radiation integral which contains the current densities given by MECA. As a consequence, our approach extends James's results to the three-dimensional case and to non-PEC scatterers. Moreover, our analytical development considers both zero and non-zero wedge angles. These differences are particularly crucial when comparing our proposed method to the PO correction techniques developed in [3, 11], which are also based on comparisons with the GTD formulation. Namely, the methods reported in [3, 11] were derived for a two-dimensional PEC diffraction problem with normal incidence at the edge, and the corresponding diffraction analyses are restricted to the case which corresponds to zero wedge angle. As we will see, the correction factors in [3] are particular cases of our correction technique.

This paper has been divided as follows. Section 2 explains the edge-fixed coordinate system used in the wedge diffraction calculations throughout the paper. In Section 3, the SPM is employed as mentioned above to calculate the asymptotic contribution of the integration boundary along the diffraction edge. Afterwards, a mathematical comparison between the analytical SPM results and the GTD formulation is performed in Section 4. The wedge diffraction correction matrix for MECA is extracted from this comparison. Section 5 includes results obtained through simulations. Finally, Section 6 concludes the paper with a summary. The manuscript contains as well one appendix with additional equations.

2. EDGE-FIXED COORDINATE SYSTEM

For the diffraction analysis presented in this paper, a flat surface with one vertex situated at the origin of a Cartesian coordinate system, as seen in Fig. 1, has been considered. The location of the origin is relevant regarding the application of the SPM as described in Section 3. The SPM is applied to one face of a wedge, which has an interior angle of α. The unit vector $\hat{\mathbf{z}}$ is tangential to the edge of this studied wedge, and $\hat{\mathbf{y}}$ is the surface normal vector. Note that the direction of $\hat{\mathbf{z}}$ should be such that $\hat{\mathbf{x}}$ is directed toward the interior of the considered surface as shown in Fig. 1. We assume that a homogeneous plane wave is incident at the interface. The incident electric field is decomposed into

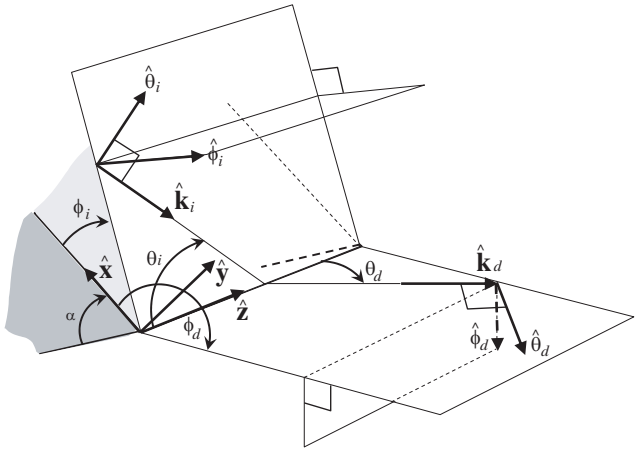

Figure 1. Edge-fixed coordinate system. θ_i is an angle subtended between the incidence direction vector $\hat{\mathbf{k}}_\mathbf{i}$ and the considered edge. θ_d is an angle between the direction of observation $\hat{\mathbf{k}}_\mathbf{d}$ and the edge. ϕ_i (ϕ_d) is the angle between the surface where we apply the three-dimensional SPM and the plane containing $\hat{\mathbf{z}}$ and the unit vector $\hat{\mathbf{k}}_\mathbf{i}$ ($\hat{\mathbf{k}}_\mathbf{d}$). α is the interior wedge angle.

two components parallel and perpendicular to the edge-fixed plane of incidence; that is, the plane containing $\hat{\mathbf{z}}$ and the unit vector $\hat{\mathbf{k}}_\mathbf{i}$ which defines the direction of incidence. Similarly, the diffracted field components are parallel and perpendicular to the edge-fixed plane of diffraction; that is, the plane containing $\hat{\mathbf{z}}$ and the unit vector $\hat{\mathbf{k}}_\mathbf{d}$ which denotes the direction of observation.

The edge-fixed Cartesian coordinate system (x, y, z) is shown in Fig. 1. The incident electric field is resolved into $\hat{\phi}_i$ and $\hat{\theta}_i$ components, and the diffracted field into $\hat{\phi}_d$ and $\hat{\theta}_d$ components, where

$$\hat{\phi}_i = \frac{-\hat{\mathbf{z}} \times \hat{\mathbf{k}}_\mathbf{i}}{\left|\hat{\mathbf{z}} \times \hat{\mathbf{k}}_\mathbf{i}\right|},\ \hat{\theta}_i = \hat{\phi}_i \times \hat{\mathbf{k}}_\mathbf{i},\ \hat{\phi}_d = \frac{\hat{\mathbf{z}} \times \hat{\mathbf{k}}_\mathbf{d}}{\left|\hat{\mathbf{z}} \times \hat{\mathbf{k}}_\mathbf{d}\right|},\ \hat{\theta}_d = \hat{\phi}_d \times \hat{\mathbf{k}}_\mathbf{d}. \qquad (1)$$

The preceding vector equations refer to conventional spherical coordinate systems relative to the diffraction edge. The unit vectors in (1) are not clearly defined when $\theta_i \to 0$. This situation leads to other important problems, notably a violation of the approximations upon which the GTD is based [12].

The angles θ_i, ϕ_i and ϕ_d shown in Fig. 1 can be determined

analytically as follows:

$$\begin{aligned}
&\theta_i = \arccos(\hat{\mathbf{k}}_\mathbf{i} \cdot \hat{\mathbf{z}});\\
&\hat{\mathbf{k}}_\mathbf{i}^\mathbf{t} = \frac{\hat{\mathbf{k}}_\mathbf{i} - (\hat{\mathbf{k}}_\mathbf{i} \cdot \hat{\mathbf{z}})\hat{\mathbf{z}}}{\left|\hat{\mathbf{k}}_\mathbf{i} - \left(\hat{\mathbf{k}}_\mathbf{i} \cdot \hat{\mathbf{z}}\right)\hat{\mathbf{z}}\right|}, \quad \hat{\mathbf{k}}_\mathbf{d}^\mathbf{t} = \frac{\hat{\mathbf{k}}_\mathbf{d} - \left(\hat{\mathbf{k}}_\mathbf{d} \cdot \hat{\mathbf{z}}\right)\hat{\mathbf{z}}}{\left|\hat{\mathbf{k}}_\mathbf{d} - \left(\hat{\mathbf{k}}_\mathbf{d} \cdot \hat{\mathbf{z}}\right)\hat{\mathbf{z}}\right|};\\
&\phi_i = \pi\left[1 - \operatorname{sgn}\left(-\hat{\mathbf{k}}_\mathbf{i}^\mathbf{t} \cdot \hat{\mathbf{y}}\right)\right] + \arccos\left(-\hat{\mathbf{k}}_\mathbf{i}^\mathbf{t} \cdot \hat{\mathbf{x}}\right) \operatorname{sgn}\left(-\hat{\mathbf{k}}_\mathbf{i}^\mathbf{t} \cdot \hat{\mathbf{y}}\right),\\
&\phi_d = \pi\left[1 - \operatorname{sgn}\left(\hat{\mathbf{k}}_\mathbf{d}^\mathbf{t} \cdot \hat{\mathbf{y}}\right)\right] + \arccos\left(\hat{\mathbf{k}}_\mathbf{d}^\mathbf{t} \cdot \hat{\mathbf{x}}\right) \operatorname{sgn}\left(\hat{\mathbf{k}}_\mathbf{d}^\mathbf{t} \cdot \hat{\mathbf{y}}\right),
\end{aligned} \tag{2}$$

with $0 \leq \arccos(u) \leq \pi$ and

$$\operatorname{sgn}(u) = \begin{cases} 1, & \text{if} \quad u \geq 0,\\ -1, & \text{if} \quad u < 0. \end{cases} \tag{3}$$

3. SPM APPLIED TO A RADIATION INTEGRAL WITH THE MECA CURRENTS

According to the MECA method [1], the equivalent magnetic and electric current densities over the flat surface are calculated by the following two equations respectively:

$$\begin{aligned}
\mathbf{M} &= \left[E^i_{\mathrm{TE}}(1+R_{\mathrm{TE}})\,(\hat{\mathbf{e}}_\mathbf{TE} \times \hat{\mathbf{n}}) + E^i_{\mathrm{TM}} \cos\theta_{inc}(1+R_{\mathrm{TM}})\,\hat{\mathbf{e}}_\mathbf{TE}\right] e^{-jk_1 \hat{\mathbf{k}}_\mathbf{i}\mathbf{r}},\\
\mathbf{J} &= \frac{1}{\eta_1}\left[E^i_{\mathrm{TE}} \cos\theta_{inc}(1-R_{\mathrm{TE}})\hat{\mathbf{e}}_\mathbf{TE} + E^i_{\mathrm{TM}}(1-R_{\mathrm{TM}})(\hat{\mathbf{n}} \times \hat{\mathbf{e}}_\mathbf{TE})\right] e^{-jk_1 \hat{\mathbf{k}}_\mathbf{i}\mathbf{r}},
\end{aligned} \tag{4}$$

where η_1 and k_1 denote respectively the impedance and the wave number in the medium of incidence. $R_{\mathrm{TE}}\,(R_{\mathrm{TM}})$ is the TE (TM) reflection coefficient for the electric field. The expressions for R_{TE} and R_{TM} can be found in [1, 13]. In order to deduce (4) in [1], the Snell reflection coefficients establish the relation between incident and reflected waves for each separate TE/TM polarization. The decomposition into TE and TM components is essential, as indicated by polarization-dependent reflection coefficients. This distinction is often not made in the literature when extending the physical optics to non-PEC objects. As shown in Fig. 2, $\mathbf{E}^\mathbf{i}_\mathbf{TE} = E^i_{\mathrm{TE}} e^{-jk_1 \hat{\mathbf{k}}_\mathbf{i} \cdot \mathbf{r}} \hat{\mathbf{e}}_\mathbf{TE}$ and $\mathbf{E}^\mathbf{i}_\mathbf{TM} = E^i_{\mathrm{TM}} e^{-jk_1 \hat{\mathbf{k}}_\mathbf{i} \cdot \mathbf{r}} \hat{\mathbf{e}}_\mathbf{TM}$ are the TE and TM components of the incident electric field at $\mathbf{r} = (x, 0, z)$, which is a position vector to any point on the scattering surface. θ_{inc} represents the angle of incidence between $\hat{\mathbf{k}}_\mathbf{i}$ and the outward unit normal vector $\hat{\mathbf{n}}$ (let us assume without loss of generality that $0 \leq \phi_i \leq \pi$ for the wedge face on which we apply the SPM).

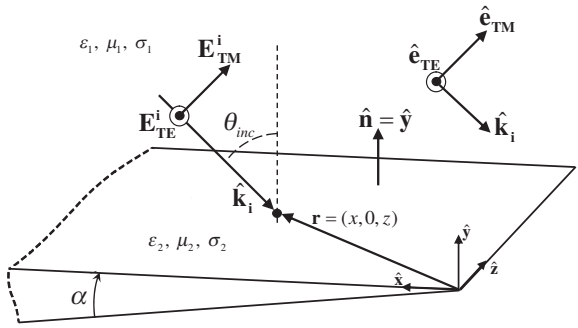

Figure 2. Oblique wave incidence on a wedge face. The first medium (medium of incidence) is characterized by its constitutive parameters: permittivity ε_1, permeability μ_1 and conductivity σ_1. Similarly, the second medium (scatterer) is characterized by (ε_2, μ_2, σ_2).

The direction of incidence is given by

$$\hat{\mathbf{k}}_{\mathbf{i}} = -\sin\theta_i \cos\phi_i \hat{\mathbf{x}} - \sin\theta_i \sin\phi_i \hat{\mathbf{y}} + \cos\theta_i \hat{\mathbf{z}}. \tag{5}$$

In terms of the notation of Figs. 1 and 2, the following substitutions can be performed in (4):

$$\hat{\mathbf{n}} = \hat{\mathbf{y}}, \quad \hat{\mathbf{e}}_{\mathbf{TE}} = \frac{\hat{\mathbf{k}}_{\mathbf{i}} \times \hat{\mathbf{y}}}{\left|\hat{\mathbf{k}}_{\mathbf{i}} \times \hat{\mathbf{y}}\right|}, \quad \cos\theta_{inc} = -\hat{\mathbf{y}} \cdot \hat{\mathbf{k}}_{\mathbf{i}} = \sin\theta_i \sin\phi_i. \tag{6}$$

In order to express (4) as a function of the components of the incident electric field along $\hat{\phi}_i$ and $\hat{\theta}_i$, as required to compare with the three-dimensional GTD formulation, the following transformation is made:

$$\begin{pmatrix} E^i_{\mathrm{TM}} \\ E^i_{\mathrm{TE}} \end{pmatrix} = \frac{1}{\sqrt{1-\sin^2\theta_i \sin^2\phi_i}} \begin{pmatrix} \cos\theta_i \sin\phi_i & \cos\phi_i \\ -\cos\phi_i & \cos\theta_i \sin\phi_i \end{pmatrix} \begin{pmatrix} E^i_{\theta_i} \\ E^i_{\phi_i} \end{pmatrix}. \tag{7}$$

Following an analogous procedure to that used in Chapter 2 of [3] for the volume integration, the scattered electric field phasor $\mathbf{E^S}$ can be written as (see also (1) in [11])

$$\mathbf{E^S} = -\frac{j}{2\lambda} \int_{S_0} \left\{ \mathbf{M} \times \hat{\mathbf{R}} + \eta_1 \left[\mathbf{J} - \left(\mathbf{J} \cdot \hat{\mathbf{R}} \right) \hat{\mathbf{R}} \right] \right\} \frac{e^{-jk_1 R}}{R} dS, \tag{8}$$

where R is the distance from a source point on the scatterer to the observation point at $h\,\hat{\mathbf{k}}_{\mathbf{d}}$ and $\hat{\mathbf{R}}$ denotes the unit vector in this

direction. The variable h is the distance from the origin to the observation point. The following equations are satisfied:

$$\begin{aligned}\mathbf{R} &= R\hat{\mathbf{R}} = h\,\hat{\mathbf{k}}_{\mathbf{d}} - x\hat{\mathbf{x}} - z\hat{\mathbf{z}} = \\ &= (h\sin\theta_d\cos\phi_d - x)\hat{\mathbf{x}} + h\sin\theta_d\sin\phi_d\hat{\mathbf{y}} + (h\cos\theta_d - z)\hat{\mathbf{z}}, \\ R &= |\mathbf{R}| = \sqrt{h^2+x^2+z^2-2h(z\cos\theta_d + x\sin\theta_d\cos\phi_d)},\ \hat{\mathbf{R}} = \mathbf{R}/R.\end{aligned} \tag{9}$$

Equation (8) is valid for $k_1 R \gg 1$, which means that the distance between the source and the observation point is much greater than the wavelength, but this assumption has no implications regarding the dimensions of the scatterer. The integral in (8) can be rewritten as

$$\mathbf{E^S} = -\frac{j}{2\lambda}\iint\limits_{S_0} \mathbf{F}(x,z)\frac{e^{jk_1 f(x,z)}}{R(x,z)}dx\,dz, \tag{10}$$

where $\mathbf{F}(x, z)$ is a vector function which includes all the vector operations in (8), $R(x, z)$ is given by (9), and the phase function $f(x, z)$ can be expressed as

$$f(x,z) = -(\hat{\mathbf{k}}_{\mathbf{i}}\cdot\mathbf{r} + R) = x\sin\theta_i\cos\phi_i - z\cos\theta_i - R(x,z). \tag{11}$$

As inferred from Subsection 3.2 of [7] (see also [8]), the critical boundary points along the diffraction edge must satisfy

$$\left.\frac{\partial f(x,z)}{\partial z}\right|_{x=0} = 0. \tag{12}$$

In our case, these critical points are of the form $(0, 0, z_C)$. Moreover, since our goal is to compare with the GTD formulation, we impose $\theta_d = \theta_i$. This condition corresponds to the Keller's cone in the GTD. Accordingly, we find that

$$\left.\frac{\partial f(x,z)}{\partial z}\right|_{x=0} = -\cos\theta_i - \frac{z - h\cos\theta_i}{\sqrt{h^2+z^2-2hz\cos\theta_i}} = 0. \tag{13}$$

The above equation has a unique solution $z_C = 0$. It should be noted that, although we obtain a critical boundary point at a vertex, this point represents the contribution of the entire diffraction edge as explained in Subsection 3.3 of [7]. The contribution of the boundary point to the radiation integral is performed by calculating the following expression [3, 7, 8]:

$$\begin{aligned}\mathbf{E^d_{SPM}} = {} & \frac{\mathbf{F}(0,z_C)}{4\pi R}e^{jk_1 f(0,z_C)} \\ & \left(\left.\frac{\partial f(x,z)}{\partial x}\right|_{x=0,z=z_C}\right)^{-1}\sqrt{\frac{2j\pi}{k_1}\left(\left.\frac{\partial^2 f(x,z)}{\partial z^2}\right|_{x=0,z=z_C}\right)^{-1}}.\end{aligned} \tag{14}$$

The asymptotic approximation of (14) is valid when the value v_0 from Equation (12) of [7] is greater than 3, i.e., $v_0 > 3$. We have checked that in the case analyzed in this paper $v_0 \propto \sqrt{k_1 h}$ so the approximation is valid in the absolute far field. Substituting the values of the derivatives in (14) yields

$$\mathbf{E}^{\mathbf{d}}_{\mathbf{SPM}} = \frac{\mathbf{F}(0, z_C)}{(\cos\phi_d + \cos\phi_i)\sin^2\theta_i} \frac{e^{-jk_1 h}}{\sqrt{8j\pi k_1 h}}. \tag{15}$$

As described in Subsection 2.2 of [14] (for the two-dimensional case), the field $\mathbf{E}^{\mathbf{d}}_{\mathbf{SPM}}$ we have obtained in (15) represents a geometrical-optic component. Evaluating $\mathbf{F}(0, z_C)$ and calculating its projections onto $\hat{\phi}_d$ and $\hat{\theta}_d$, it is possible to write (15) in the form

$$\begin{pmatrix} E^{d,\mathrm{SPM}}_{\theta_d} \\ E^{d,\mathrm{SPM}}_{\phi_d} \end{pmatrix} = \begin{pmatrix} D^{\mathrm{SPM}}_{11} & D^{\mathrm{SPM}}_{12} \\ D^{\mathrm{SPM}}_{21} & D^{\mathrm{SPM}}_{22} \end{pmatrix} \begin{pmatrix} E^{i}_{\theta_i} \\ E^{i}_{\phi_i} \end{pmatrix} \frac{e^{-jk_1 h}}{\sqrt{8j\pi k_1 h}}. \tag{16}$$

The elements of the matrix in the previous equation can be found in Appendix A. As commented above, we identify (16) as diffracted GO (geometrical optics) field. In the next section, the diffraction coefficients in the matrix of (16) are compared to the GTD in order to correct (16).

4. WEDGE DIFFRACTION CORRECTION MATRIX

In [15], Luebbers modified Keller's PEC GTD [16] to include finite conductivity and the effects of relative permittivity on GTD fields. The two-dimensional GTD coefficients of Luebbers [15] have recently been extended to the three-dimensional case in [17]. These extended coefficients depend on the angles in (2) and on the constitutive parameters of the scattering material, and can be expressed in matrix form as

$$\begin{pmatrix} E^{d,\mathrm{GTD}}_{\theta_d} \\ E^{d,\mathrm{GTD}}_{\phi_d} \end{pmatrix} = \begin{pmatrix} D^{\mathrm{GTD}}_{11} & D^{\mathrm{GTD}}_{12} \\ D^{\mathrm{GTD}}_{21} & D^{\mathrm{GTD}}_{22} \end{pmatrix} \begin{pmatrix} E^{i}_{\theta_i} \\ E^{i}_{\phi_i} \end{pmatrix} \frac{e^{-jk_1 h}}{\sqrt{8j\pi k_1 h}}. \tag{17}$$

Again, the expressions for the GTD diffraction coefficients in the preceding matrix are included in Appendix A.

Comparing (16) and (17), we can multiply the incident field in (16) by a wedge diffraction correction matrix C such that

$$\begin{pmatrix} D^{\mathrm{SPM}}_{11} & D^{\mathrm{SPM}}_{12} \\ D^{\mathrm{SPM}}_{21} & D^{\mathrm{SPM}}_{22} \end{pmatrix} \underbrace{\begin{pmatrix} C_{11} & C_{12} \\ C_{21} & C_{22} \end{pmatrix}}_{C} \begin{pmatrix} E^{i}_{\theta_i} \\ E^{i}_{\phi_i} \end{pmatrix} = \begin{pmatrix} D^{\mathrm{GTD}}_{11} & D^{\mathrm{GTD}}_{12} \\ D^{\mathrm{GTD}}_{21} & D^{\mathrm{GTD}}_{22} \end{pmatrix} \begin{pmatrix} E^{i}_{\theta_i} \\ E^{i}_{\phi_i} \end{pmatrix}. \tag{18}$$

The correction matrix C transforms the diffracted GO component deduced from MECA through the stationary phase method, into a GTD component.

Note that the SPM allows us to mathematically obtain matrix C; however, the SPM is not applied in the computational code where the diffraction correction matrix C is implemented. Unfortunately, the equations for the explicit elements of the correction matrix are much too complicated to be worth writing down here. Let us emphasize that this fact is not a problem for computational implementation purposes, since matrix C can be easily obtained numerically from the other 2×2 matrices in (18). Nevertheless, we can present novel analytical expressions for particular cases of interest.

A rectangular perfectly conducting plate has all its wedge angles of size $\alpha = 0$, and is infinitely thin. Consequently, in case of a PEC plate, it is always true that $R_{\mathrm{TE}} = R_{\mathrm{TM}} = R^s_{0,n} = R^h_{0,n} = -1$, $n = 2$. Let us remark that R_{TE} and R_{TM} are respectively the TE and TM reflection coefficients for the electric field, introduced in Section 3. Additionally, $R^s_{0,n}$ and $R^h_{0,n}$ are, as shown in Appendix A, the soft and hard reflection coefficients, respectively, incorporated into the GTD diffraction coefficients (R_{TM} and $R^h_{0,n}$ refer here to the *electric* field reflection, so their value is not 1). The parameter n is given by (A11) in Appendix A. In the geometry discussed here, for every edge, matrix C is obtained by substituting the particular values addressed in this paragraph into the coefficients of (16) and (17), and then solving (18). In this particular case, matrix C becomes

$$C = \begin{pmatrix} \sec(\phi_i/2)\sin(\phi_d/2) & \\ 0 & \\ -\frac{1}{2}\cos(\theta_i)[\cos(\phi_d)+\cos(\phi_i)]\csc(\phi_d/2)\csc(\phi_i/2) & \\ \cos(\phi_i/2)\csc(\phi_d/2) & \end{pmatrix}. \quad (19)$$

At normal incidence relative to the considered edge ($\theta_i = \pi/2$) and if the scatterer is not necessarily composed of PEC material, then the elements of matrix C reduce to

$$C_{11} = \frac{[\cos(\phi_d)+\cos(\phi_i)]\left[R^s_0 \cot\left(\frac{\pi-(\phi_d+\phi_i)}{2n}\right)+R^s_n \cot\left(\frac{\pi+(\phi_d+\phi_i)}{2n}\right)\right.}{\left.+\cot\left(\frac{\pi+(\phi_d-\phi_i)}{2n}\right)+\cot\left(\frac{\pi-(\phi_d-\phi_i)}{2n}\right)\right]} \\ n[(1+R_{\mathrm{TE}})\sin(\phi_d)-(1-R_{\mathrm{TE}})\sin(\phi_i)],$$

$$C_{22}=\frac{\begin{array}{c}[\cos(\phi_d)+\cos(\phi_i)]\Bigg[R_0^h\cot\left(\dfrac{\pi-(\phi_d+\phi_i)}{2n}\right)+R_n^h\cot\left(\dfrac{\pi+(\phi_d+\phi_i)}{2n}\right)\\ -\cot\left(\dfrac{\pi+(\phi_d-\phi_i)}{2n}\right)-\cot\left(\dfrac{\pi-(\phi_d-\phi_i)}{2n}\right)\Bigg]\end{array}}{n[(1+R_{\mathrm{TM}})\sin(\phi_i)-(1-R_{\mathrm{TM}})\sin(\phi_d)]}, \tag{20}$$

$$C_{12}=C_{21}=0.$$

If we take $\theta_i=\pi/2$ in (19), or $n=2$ and $R_{\mathrm{TE}}=R_{\mathrm{TM}}=R_{0,n}^s=R_{0,n}^h=-1$ in (20), we obtain as expected a diagonal matrix whose elements are exactly the correction factors explained in Section 5.6 of [3] for the two-dimensional PEC half-plane case. The expressions of these factors, which can be deduced as a particular case of the results in the present paper, were also published in Section 3 of [18].

5. IMPLEMENTATION AND SIMULATION RESULTS

In the computational implementation of MECA described in [1], the surface radiation integral is decomposed into the contributions from planar triangular facets. The currents are assumed to have constant amplitude and linear phase variation on every facet. In the present work, we utilize the same approach of discretizing into planar triangular facets. Therefore we only apply the correction matrix to the incident electric field on those facets which have one side coincident with the portion of an edge. In order to obtain the results presented in this section, we developed a parallel implementation of MECA in which the optimization techniques explained in [19] were applied.

Before multiplying by the correction matrix, the unit vectors in (1) must be computed in order to resolve the incident field into $\hat{\phi}_i$ and $\hat{\theta}_i$ components, and the angles in (2) must be determined in order to evaluate the correction matrix. Equations (1) and (2) are calculated once for each edge. The diffraction correction is only implemented for the incident electric field terms in those radiation integrals belonging to one face of each wedge; otherwise, the GTD fields would be included twice in the MECA method. Since the GTD fields are confined to the Keller's cone, for each given triangular facet, the matrix multiplication correction is solely applied if the observation direction lies in the Keller's cone relative to the considered facet. This condition can be expressed as

$$\left(\hat{\mathbf{k}}_{\mathbf{d}}-\hat{\mathbf{k}}_{\mathbf{i}}\right)\cdot\hat{\mathbf{e}}=0, \tag{21}$$

where the unit vector $\hat{\mathbf{k}}_{\mathbf{d}}$ defines the direction of observation, $\hat{\mathbf{k}}_{\mathbf{i}}$ is the direction of incidence, and $\hat{\mathbf{e}}$ is a vector parallel to the facet side

(portion of an edge) at which diffraction occurs. This restriction to the Keller's cone is frequently taken into account in the related literature. (For instance, see the diffraction integrals in the recent reference [20].)

A comparison in terms of scattered far-field computations validates the diffraction correction method presented in this paper using simulated full-wave results of canonical geometries. These simulated results deal with different types of surfaces ranging from PEC to dielectric materials and including lossy cases which have not been previously considered in other PO diffraction correction techniques such as those described in [3, 9–11].

5.1. Square Flat PEC Plate

The first validation geometry consists of a square flat PEC plate whose length is 3 cm, located in the XY plane. (Note that, in this section, we are referring to a global coordinate system — different from that of Section 2 — where here $\hat{\mathbf{z}}$ is the surface normal vector.) Figs. 3 and 4 show comparisons among the far-field patterns obtained by MoM, original MECA and a modified version of MECA which includes the diffraction correction described in this paper.

The incident electric field on the PEC plate is a plane wave polarized along the $\hat{\theta}$ direction, with amplitude 1 V/m, and $f = 94$ GHz. The results in Fig. 3 correspond to normal incidence on the interface, whereas oblique incidence angles of $\theta_{inc} = 30°$ and $\theta_{inc} = 45°$ have been introduced in order to obtain the patterns presented in

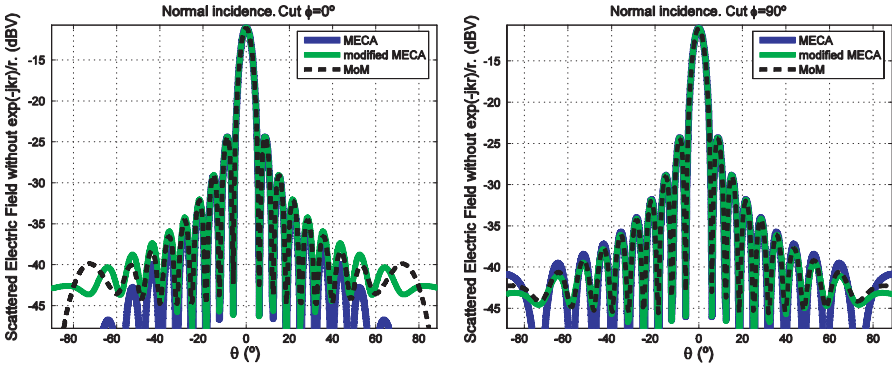

Figure 3. Comparison at a frequency of 94 GHz among different solutions along the observation cuts $\phi = 0°$ (a) and $\phi = 90°$ (b) for a square PEC scatterer of side length 3 cm, with normal plane wave incidence.

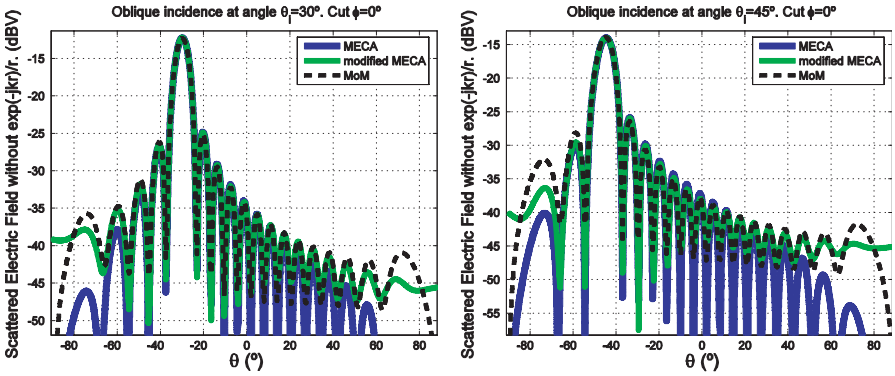

Figure 4. Comparison at a frequency of 94 GHz among different solutions along the observation cut $\phi = 0°$ for a square PEC scatterer of side length 3 cm, with oblique plane wave incidence at $\theta_{inc} = 30°$ (a) and $\theta_{inc} = 45°$ (b).

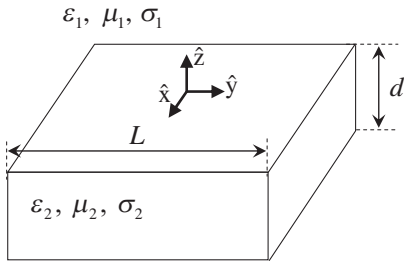

Figure 5. Cuboidal slab of thickness d and square face with side length L.

Fig. 4. It can be observed that the overlap between the MECA and MoM curves is improved when the diffraction correction technique is incorporated into MECA.

5.2. Cuboidal Penetrable Slab

The next set of examples consists of a cuboidal penetrable slab whose thickness d is large compared to the penetration depth of the material at the simulation frequency. A plane wave whose electric field is polarized along $\hat{\mathbf{x}}$, with amplitude 1 V/m, impinges at normal incidence on a square face of the slab. The value of the side length L of this incidence face, indicated in Fig. 5, was set to be 3 m.

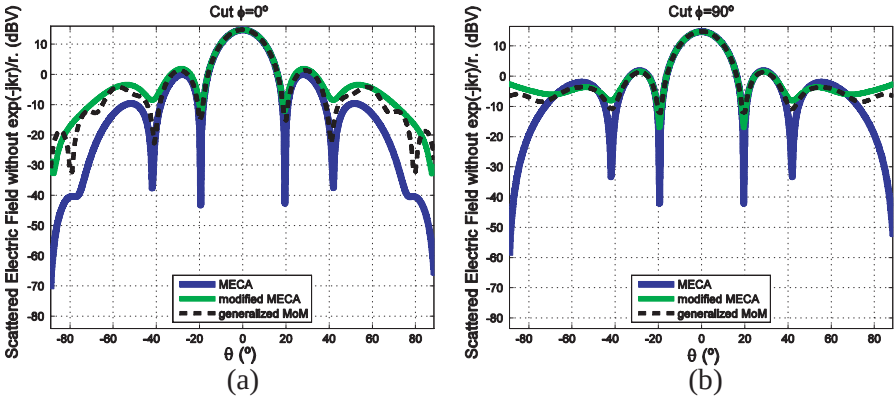

Figure 6. Comparison at a frequency of 300 MHz among different solutions along the observation cuts $\phi = 0°$ (a) and $\phi = 90°$ (b) for a dielectric slab with $\varepsilon_2 = 15\varepsilon_0$ and $\sigma_2 = 0.1\,\mathrm{S/m}$.

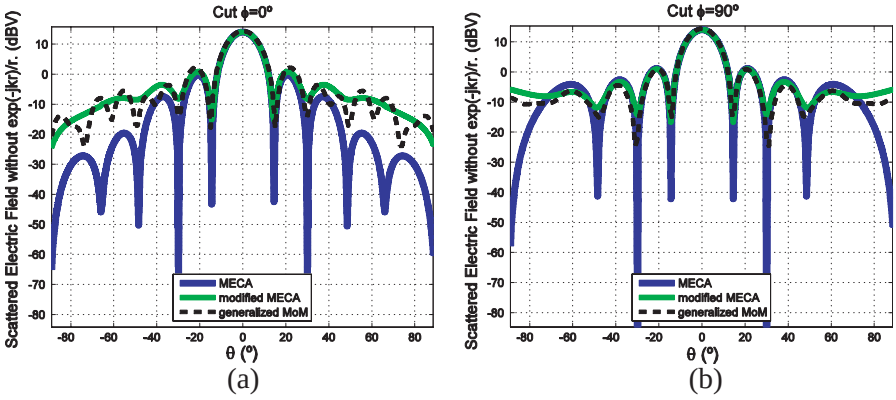

Figure 7. Comparison at a frequency of 400 MHz among different solutions along the observation cuts $\phi = 0°$ (a) and $\phi = 90°$ (b) for a dielectric slab with $\varepsilon_2 = 6\varepsilon_0$ and $\sigma_2 = 0.005\,\mathrm{S/m}$.

Two cases have been considered: a general lossy dielectric medium ($\varepsilon_2 = 15\varepsilon_0$, $\sigma_2 = 0.1\,\mathrm{S/m}$, $f = 300\,\mathrm{MHz}$) in Fig. 6 and a good dielectric ($\varepsilon_2 = 6\varepsilon_0$, $\sigma_2 = 0.005\,\mathrm{S/m}$, $f = 400\,\mathrm{MHz}$) in Fig. 7. The full-wave solution, taken as reference, has been obtained from a version of MoM for penetrable scatterers. A description of this generalized formulation of MoM can be found in [21].

For a cuboidal slab, the parameter n given by (A11) in Appendix A has the value 3/2 for every wedge since the interior angles measure 90°.

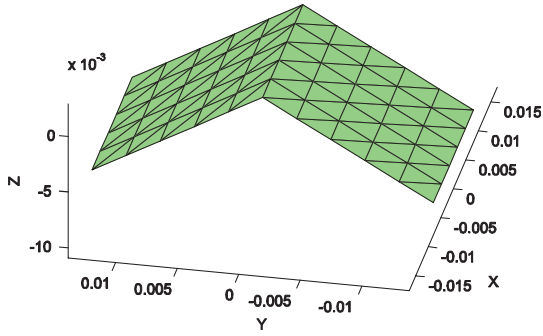

Figure 8. Geometry of the dihedral corner reflector formed by two square PEC plates each 5λ long. In this case, the maximum leg length of the mesh triangles for the MECA simulations was set to λ, as shown in this figure, whereas for the MoM simulation was $\lambda/10$.

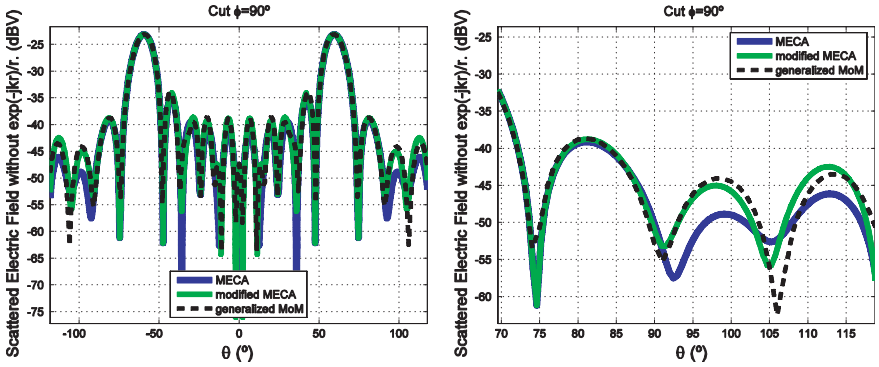

Figure 9. Comparison at a frequency of 94 GHz among different solutions along the observation cut $\phi = 90°$ for a dihedral corner reflector composed of two square PEC plates of side length 5λ, with an interior wedge angle $\alpha = 120°$. The curves on the right correspond to a zoom-in on an area over the graph on the left, around the grazing observation direction for one of the plates.

The inclusion of the GTD parameter n is a major difference compared to the GTD-based PO-correction techniques proposed in [3, 11], which are limited to the case $n = 2$ and only restricted to PEC scatterers. On the evidence of the results presented in Figs. 6 and 7, it can be inferred that our proposed method can efficiently approximate the envelopes of the MoM curves due to non-PEC scatterers.

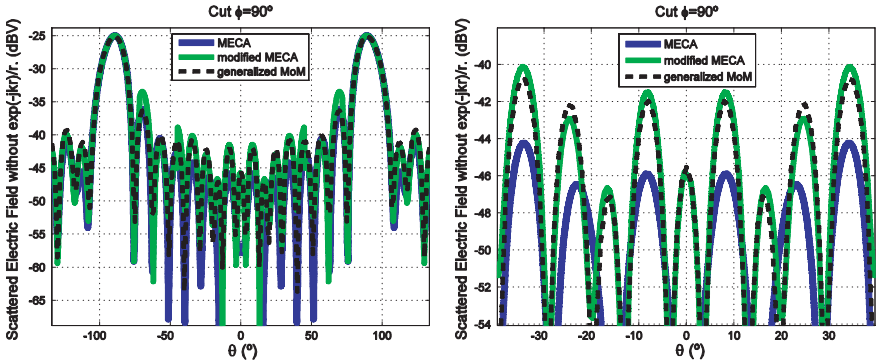

Figure 10. Comparison at a frequency of 94 GHz among different solutions along the observation cut $\phi = 90°$ for a dihedral corner reflector composed of two square PEC plates of side length 5λ, with an interior wedge angle $\alpha = 90°$. The curves on the right correspond to a zoom-in on an area over the graph on the left, around the central direction of observation.

5.3. Dihedral Corner Reflector

The dihedral corner reflector is useful for evaluating the field contributions caused by diffraction at arbitrary wedge angles. The simulated geometry is composed of two square PEC plates each 5λ long so the dihedral axis is along the Z-axis and the angle between each plate and the XZ plane is $\alpha/2$. This geometry is depicted in Fig. 8 together with the triangular mesh of the surfaces employed in MECA. The origin of the global Cartesian system is situated at the dihedral vertex. The incident electric field consists of a plane wave polarized along the $\hat{\mathbf{y}}$ direction, with amplitude 1 V/m, $f = 94$ GHz and incidence direction $-\hat{\mathbf{z}}$. In order to highlight the wedge diffraction effects on simulation results, we have chosen that the wavefront impinges on the convex dihedral angle. In the concave dihedral angle, the effects of multiple reflections between plates would dominate over wedge diffraction contributions.

Figures 9 and 10 present the far-field distributions obtained by simulation of the scattering from a dihedral corner reflector using MoM, MECA, and a version of MECA modified with the proposed correction technique. The angle between the plates (interior wedge angle) was $\alpha = 120°$ for the patterns in Fig. 9 and $\alpha = 90°$ for those in Fig. 10. Both examples show a good agreement between modified MECA and MoM results in the given angular margin.

6. CONCLUSION

This paper presents a technique for correcting the wedge diffraction contributions in a modified PO method, known as the modified equivalent current approximation (MECA) method, valid for both PEC and dielectric objects. We have extended the analytical results in [3] to the three-dimensional case, to non-PEC scatterers, and to non-zero wedge angles. The correction matrix is derived comparing the GTD diffracted fields with the diffraction component obtained through the three-dimensional stationary phase method.

Regarding the scope of application, the main difference between our technique and the general three-dimensional GTD published in [17] concerns the fact that our proposed technique is directly applicable to the PO and MECA formulations.

Our simulation data show that the coincidence between the results provided by a computational implementation of MECA and a full-wave MoM method is increased by applying the wedge diffraction correction matrix technique.

ACKNOWLEDGMENT

This work was partially supported by the Spanish Government, Xunta de Galicia and ERDF funds under projects: TEC2011-28683-C02-02, INCITE08PXIB322219PR, CSD2008-00068, program "Ramón y Cajal" RYC-2009-04924, and Consolidation of Research Units in Galicia 2008/075. H. Gómez-Sousa acknowledges support from the predoctoral fellowship PRE/2011/152 of the "Plan Galego de Investigación, Innovación e Crecemento 2011-2015 (Plan I2C)" from Xunta de Galicia. The authors thank the staff of the "Centro de Supercomputación de Galicia" (CESGA) for providing access to the supercomputer FinisTerrae.

APPENDIX A. SPM AND GTD DIFFRACTION COEFFICIENTS

This appendix contains the coefficients D_{ij}^{SPM} of the matrix obtained through the SPM procedure presented in Section 3, and the general expressions for the GTD diffraction coefficients $D_{ij}^{\mathrm{GTD}}$of the matrix in Section 4.

The elements of the matrix in (16) represent the SPM diffraction coefficients which can be found by applying the version of the SPM published in [7, 8], and by performing the manipulations described in

Section 3 of this paper. These coefficients are given by:

$$D_{11}^{\mathrm{SPM}}=\left.\frac{E_{\theta_d}^d}{E_{\theta_i}^i}\right|_{E_{\phi_i}^i=0}=\frac{1}{\sin\theta_i(\cos\phi_d+\cos\phi_i)\left(1-\sin^2\theta_i\sin^2\phi_i\right)}\cdot[(1+R_{\mathrm{TE}})$$
$$\cos^2\phi_i\sin\phi_d+(1-R_{\mathrm{TE}})\sin\phi_i\cos\phi_i\left(\cos^2\theta_i\cos\phi_d-\cos\phi_i\sin^2\theta_i\right)+(1+R_{\mathrm{TM}})$$
$$\sin^2\phi_i\cos^2\theta_i\sin\phi_d-(1-R_{\mathrm{TM}})\sin\phi_i\cos^2\theta_i(1+\cos\phi_i\cos\phi_d)],\quad\text{(A1)}$$

$$D_{22}^{\mathrm{SPM}}=\left.\frac{E_{\phi_d}^d}{E_{\phi_i}^i}\right|_{E_{\theta_i}^i=0}=\frac{1}{\sin\theta_i(\cos\phi_d+\cos\phi_i)\left(1-\sin^2\theta_i\sin^2\phi_i\right)}\cdot[-(1+R_{\mathrm{TE}})$$
$$\sin\phi_i\cos^2\theta_i(1+\cos\phi_i\cos\phi_d)+(1-R_{\mathrm{TE}})\sin^2\phi_i\cos^2\theta_i\sin\phi_d+(1+R_{\mathrm{TM}})$$
$$\sin\phi_i\cos\phi_i\left(\cos^2\theta_i\cos\phi_d-\cos\phi_i\sin^2\theta_i\right)+(1-R_{\mathrm{TM}})\cos^2\phi_i\sin\phi_d],\quad\text{(A2)}$$

$$D_{12}^{\mathrm{SPM}}=\left.\frac{E_{\theta_d}^d}{E_{\phi_i}^i}\right|_{E_{\theta_i}^i=0}=\frac{1}{\sin\theta_i(\cos\phi_d+\cos\phi_i)\left(1-\sin^2\theta_i\sin^2\phi_i\right)}\cdot[-(1+R_{\mathrm{TE}})$$
$$\sin\phi_i\cos\phi_i\cos\theta_i\sin\phi_d-(1-R_{\mathrm{TE}})\sin^2\phi_i\cos\theta_i$$
$$\left(\cos^2\theta_i\cos\phi_d-\cos\phi_i\sin^2\theta_i\right)+(1+R_{\mathrm{TM}})\sin\phi_i\cos\phi_i\cos\theta_i\sin\phi_d$$
$$-(1-R_{\mathrm{TM}})\cos\phi_i\cos\theta_i(1+\cos\phi_i\cos\phi_d)],\quad\text{(A3)}$$

$$D_{21}^{\mathrm{SPM}}=\left.\frac{E_{\phi_d}^d}{E_{\theta_i}^i}\right|_{E_{\phi_i}^i=0}=\frac{1}{\sin\theta_i(\cos\phi_d+\cos\phi_i)\left(1-\sin^2\theta_i\sin^2\phi_i\right)}\cdot[(1+R_{\mathrm{TE}})$$
$$\cos\phi_i\cos\theta_i(1+\cos\phi_i\cos\phi_d)-(1-R_{\mathrm{TE}})\sin\phi_i\cos\phi_i\cos\theta_i\sin\phi_d+$$
$$+(1+R_{\mathrm{TM}})\sin^2\phi_i\cos\theta_i\left(\cos^2\theta_i\cos\phi_d-\cos\phi_i\sin^2\theta_i\right)$$
$$+(1-R_{\mathrm{TM}})\sin\phi_i\cos\phi_i\cos\theta_i\sin\phi_d].\quad\text{(A4)}$$

The GTD diffraction coefficients in matrix (17) are defined as follows [17]:

$$D_{11}^{\mathrm{GTD}}=\frac{1}{n\cdot\sin\theta_i\left(1-\sin^2\theta_i\sin^2\phi_i\right)}\cdot$$
$$\left\{\left(R_0^s\cos^2\phi_i+R_0^h\cos^2\theta_i\sin^2\phi_i\right)\cot\left(\frac{\pi-(\phi_d+\phi_i)}{2n}\right)+\right.$$
$$+\left(R_n^s\cos^2\phi_i+R_n^h\cos^2\theta_i\sin^2\phi_i\right)\cot\left(\frac{\pi+(\phi_d+\phi_i)}{2n}\right)$$
$$\left.+\left(1-\sin^2\theta_i\sin^2\phi_i\right)\left[\cot\left(\frac{\pi-(\phi_d-\phi_i)}{2n}\right)+\cot\left(\frac{\pi+(\phi_d-\phi_i)}{2n}\right)\right]\right\},\quad\text{(A5)}$$

$$D_{22}^{\mathrm{GTD}} = \frac{1}{n \cdot \sin\theta_i \left(1-\sin^2\theta_i \sin^2\phi_i\right)} \cdot$$
$$\left\{ -\left(R_0^h \cos^2\phi_i + R_0^s \cos^2\theta_i \sin^2\phi_i\right) \cot\left(\frac{\pi-(\phi_d+\phi_i)}{2n}\right) + \right.$$
$$- \left(R_n^h \cos^2\phi_i + R_n^s \cos^2\theta_i \sin^2\phi_i\right) \cot\left(\frac{\pi+(\phi_d+\phi_i)}{2n}\right)$$
$$\left. + \left(1-\sin^2\theta_i \sin^2\phi_i\right) \left[\cot\left(\frac{\pi-(\phi_d-\phi_i)}{2n}\right) + \cot\left(\frac{\pi+(\phi_d-\phi_i)}{2n}\right) \right] \right\}, \quad \text{(A6)}$$

$$D_{12}^{\mathrm{GTD}} = \frac{\sin\phi_i \cos\phi_i \cos\theta_i}{n \cdot \sin\theta_i \left(1-\sin^2\theta_i \sin^2\phi_i\right)} \cdot$$
$$\left[\left(R_0^h - R_0^s\right) \cot\left(\frac{\pi-(\phi_d+\phi_i)}{2n}\right) + \left(R_n^h - R_n^s\right) \cot\left(\frac{\pi+(\phi_d+\phi_i)}{2n}\right) \right], \quad \text{(A7)}$$

$$D_{21}^{\mathrm{GTD}} = -D_{12}^{\mathrm{GTD}}. \quad \text{(A8)}$$

$R_{0,n}^s$ and $R_{0,n}^h$ are the so-called soft and hard reflection coefficients, respectively, incorporated into the GTD diffraction coefficients [17]:

$$R_{0,n}^s = \frac{\sin(\theta_{0,n}) - \sqrt{\varepsilon_{cr2} - \cos^2(\theta_{0,n})}}{\sin(\theta_{0,n}) + \sqrt{\varepsilon_{cr2} - \cos^2(\theta_{0,n})}},$$
$$R_{0,n}^h = -\frac{\varepsilon_{cr2}\sin(\theta_{0,n}) - \sqrt{\varepsilon_{cr2} - \cos^2(\theta_{0,n})}}{\varepsilon_{cr2}\sin(\theta_{0,n}) + \sqrt{\varepsilon_{cr2} - \cos^2(\theta_{0,n})}}. \quad \text{(A9)}$$

In (A9) the surrounding medium is assumed to be free space with $\varepsilon_1 = \varepsilon_0$ and $\mu_1 = \mu_0$, the scatterer is supposed to have $\mu_2 = \mu_0$, and the complex relative permittivity ε_{cr2} of the scatterer is defined as

$$\varepsilon_{cr2} = \frac{1}{\varepsilon_0}\left(\varepsilon_2 - j\frac{\sigma_2}{2\pi f}\right). \quad \text{(A10)}$$

The interior wedge angle α, depicted in Figs. 1 and 2, is related to the parameter n in (A5)–(A8) by

$$n = 2 - \alpha/\pi, \quad \text{(A11)}$$

with α measured in radians. Note that n need not be an integer.

Angles θ_0 and θ_n in (A9) are calculated by using the following expressions [17]:

$$\theta_0 = \min\left(\phi_i, \phi_d\right), \quad \theta_n = \min\left(n\pi - \phi_i, n\pi - \phi_d\right). \quad \text{(A12)}$$

It should be observed that, in (A5)–(A8), the Fresnel integrals involved in the original uniform diffraction coefficients presented in [17] have been set equal to unity. As stated in Subsection V.A of [22], we

can set these Fresnel transition functions equal to unity in case of an incident plane wave if the observation point is sufficiently far from the edge. This approximation has also been applied in the PO diffraction correction technique developed in [11]. When any cotangent function in (A5)–(A8) has an argument which causes a singularity in some of the GTD coefficients, we explicitly avoid the far-field numerical evaluation for the observation direction in which the singularity occurs. This form of avoidance can be achieved because the set of simulated observation directions is a discrete sampling. From the discussion in Section 2 of [23], it follows that, for the case of an incident plane wave, the GTD solution is adequate except for a range of angles about the optical boundaries where the singularities take place. As discussed in [23], that range of angles can be made arbitrarily small by increasing the distance between the edge and the observation point. For the results of the present paper, we perform scattering calculations restricted to the far field region ($k_1 h \to \infty$). Therefore, we draw upon the approximations we have dealt with above.

REFERENCES

1. Meana, J. G., J. Á. Martínez-Lorenzo, F. Las-Heras, and C. Rappaport, "Wave scattering by dielectric and lossy materials using the modified equivalent current approximation (MECA)," *IEEE Trans. on Antennas and Propag.*, Vol. 58, No. 11, 3757–3761, 2010.
2. Meana, J. G., J. Á. Martínez-Lorenzo, F. Las-Heras, and C. Rappaport, "A PO-MoM comparison for electrically large dielectric geometries," *IEEE Antennas and Propagation Society International Symposium, APSURSI'09*, June 1–5, 2009.
3. James, G. L., *Geometrical Theory of Diffraction for Electromagnetic Waves*, Peregrinus, Stevenage, U.K., 1980.
4. Lee, S. W., "Comparison of uniform asymptotic theory and Ufimtsev's theory of electromagnetic edge diffraction," *IEEE Trans. on Antennas and Propag.*, Vol. 25, No. 2, 162–170, 1977.
5. Ufimtsev, P. Y., "Method of edge waves in the physical theory of diffraction," Air Force System Command, Foreign Tech. Div., ID No. FTD-HC-23-259-71, 1971.
6. Ufimtsev, P. Y., *Fundamentals of the Physical Theory of Diffraction*, Wiley, New Jersey, 2007.
7. Conde, O., J. Pérez, and M. F. Cátedra, "Stationary phase method application for the analysis of radiation of complex 3-D

conducting structures," *IEEE Trans. on Antennas and Propag.*, Vol. 49, No. 5, 724–731, 2001.

8. Sáez de Adana, F., et al., *Practical Applications of Asymptotic Techniques in Electromagnetics*, Artech House, 2010.
9. Umul, Y. Z., "Modified theory of physical optics," *Opt. Express*, Vol. 12, No. 20, 4959–4972, 2004.
10. Sakina, K., S. Cui, and M. Ando, "Mathematical derivation of modified edge representation for reduction of surface radiation integral," *IEICE Trans. Electron.*, Vol. E84-C, No. 1, 74–83, 2001.
11. Shijo, T., L. Rodríguez, and M. Ando, "The modified-surface normal vectors in the physical optics," *IEEE Trans. on Antennas and Propag.*, Vol. 56, No. 12, 3714–3722, 2008.
12. McNamara, D. A., C. W. I. Pistorius, and J. A. G. Malherbe, *Introduction to the Uniform Geometrical Theory of Diffraction*, Artech House, Norwood, MA, 1990.
13. Staelin, D. H., A. W. Morgenthaler, and J. A. Kong, *Electromagnetic Waves*, Prentice Hall, USA, 1994.
14. Shijo, T. and M. Ando, "Elimination of fictitious penetrating rays from PO and hybridization with AFIM," *Electrical Engineering in Japan*, Vol. 150, No. 2, 2005. [Translated from *Denki Gakkai Ronbunshi*, Vol. 123-A, No. 12, 1185–1192, Dec. 2003].
15. Luebbers, R. J., "Finite conductivity uniform GTD versus knife edge diffraction in prediction of propagation path loss," *IEEE Trans. on Antennas and Propag.*, Vol. 32, No. 1, 70–76, 1984.
16. Keller, J. B., "Geometrical theory of diffraction," *J. Opt. Soc. Amer.*, Vol. 52, 116–130, 1962.
17. Soni, S. and A. Bhattacharya, "Novel three-dimensional dyadic diffraction coefficient for wireless channel," *Microwave and Optical Technology Letters*, Vol. 52, No. 9, 2132–2136, 2010.
18. Constantinides, E. D. and R. J. Marhefka, "A UGO/EUTD solution for the scattering and diffraction from cubic polynomial strips," *IEEE Trans. on Antennas and Propag.*, Vol. 41, No. 8, 1088–1098, 1993.
19. Gómez-Sousa, H., J. Á. Martínez-Lorenzo, O. Rubiños-López, J. G. Meana, M. Graña-Varela, B. González-Valdés, and M. Arias-Acuña, "Strategies for improving the use of the memory hierarchy in an implementation of the modified equivalent current approximation (MECA) method," *ACES Journal*, Vol. 25, No. 10, 841–852, 2010.
20. Gennarelli, G. and G. Riccio, "Diffraction by a lossy double-negative metamaterial layer: A uniform asymptotic solution,"

Progress In Electromagnetics Research Letters, Vol. 13, 173–180, 2010.

21. Medgyesi-Mitschang, L. N., J. M. Putnam, and M. B. Gedera, "Generalized method of moments for three-dimensional penetrable scatterers," *J. Opt. Soc. Amer. A*, Vol. 11, No. 4, 1383–1398, 1994.
22. Kouyoumjian, R. G. and P. H. Pathak, "A uniform geometrical theory of diffraction for an edge in a perfectly-conducting surface," *Proc. IEEE*, Vol. 62, No. 11, 1448–1461, 1974.
23. Menendez, R. C. and S. W. Lee, "On the role of the geometrical optics field in aperture diffraction," *IEEE Trans. on Antennas and Propag.*, Vol. 25, No. 5, 688–695, 1977.